Sustainable 3D-printing from coconut waste: conductive PLA-biochar filaments for environmental electrochemical sensing

Raquel G. Rocha[1] · Mariana C. Marra[1] · Isabella C. O. F. Silva[1] · Gilvana P. Siqueira[1] · Robert D. Crapnell[2] · Craig E. Banks[2] · Eduardo M. Richter[1] · Rodrigo A. A. Muñoz[1]

Abstract

The integration of eco-friendly composites based on polymers and conductive fillers offers exciting opportunities for creating sustainable materials with superior electrical properties, paving the way for innovative advancements in electroanalytical devices. In this study, we explored the potential of biodegradable polylactic acid (PLA), carbon black (CB), and biochar derived from coconut shell waste to develop fused filament fabrication (FFF) filaments without the need for hazardous solvents. To assess the influence of biochar on the electrochemical properties, additional filaments composed exclusively of CB and PLA were also fabricated for comparison. The resulting conductive FFF filaments were used to fabricate additively manufactured electrodes. The biochar-CB/PLA electrode presented superior electrochemical activity, as indicated by cyclic voltammetry (CV) scans for both outer-sphere ($[Ru(NH_3)_6]^{2+/3+}$) and inner-sphere ($[Fe(CN)_6]^{3-/4-}$) redox couples. The biochar-CB/PLA electrodes also exhibited a lower charge transfer resistance ($Rct = 1.01 \pm 0.05$ kΩ) than the CB/PLA sensor ($Rct = 9.11 \pm 0.03$ kΩ), highlighting the improved performance of the conductive biochar-CB/PLA filament in the production of working electrodes. The biochar, acting as an adsorbent, enhances electrochemical performance by pre-concentrating analytes at the electrode surface. Furthermore, the biochar-CB/PLA electrodes were successfully employed to detect carbendazim (CBZ), a widely used fungicide, in environmental (lake and tap water) and food (lemon juice and drinking water) samples, using differential pulse voltammetry (DPV). A linear range of 0.1 to 5.0 µmol L^{-1} and a limit of detection (LOD) of 0.01 µmol L^{-1} were achieved for CBZ determination. Recovery values (~ 90–115%) were achieved for the analysis of samples, indicating the potential of biochar-CB/PLA-based electrodes for reliable and sustainable electrochemical sensing applications.

Keywords Additive manufacturing · Agro-industries residues · FDM technology · Food analysis · Pesticides · Differential pulse voltammetry · Water analysis

Introduction

Additive manufacturing (AM) has emerged as a powerful method for creating 3D objects layer-by-layer [1, 2]. This innovative process allows to produce components from a wide range of materials, enabling both simple and highly complex designs, with the added benefit of customization [1]. In comparison to traditional subtractive manufacturing methods such as laser cutting, turning, and water jet cutting, AM generates significantly less waste [3, 4].

Among the various AM technologies, extrusion-based methods, particularly fused filament fabrication (FFF), also known as fused deposition modeling (FDM), are especially advantageous due to their (i) cost-effectiveness, with FFF machines being up to 400 times cheaper than laser-based printers [5–7]; (ii) rapid prototyping capabilities [6, 8]; and (iii) lower energy consumption [9]. Recent studies have shown that FFF technology uses considerably less thermal energy compared to laser powder bed fusion, making it an energy-efficient alternative for additive manufacturing [5].

However, despite these advantages, FFF faces challenges, especially concerning plastic waste and the reliance on

✉ Raquel G. Rocha
raquel_rocha1793@hotmail.com

✉ Rodrigo A. A. Muñoz
munoz@ufu.br

[1] Institute of Chemistry, Federal University of Uberlândia, Uberlândia, MG 38408-100, Brazil

[2] Faculty of Science and Engineering, Manchester Metropolitan University, Dalton Building, Chester Street, Manchester M1 5GD, UK

petroleum-based polymers. To address this, several research groups have explored the use of recycled polymers [10–15]. For example, Sigley et al. [16] demonstrated the integration of circular economy principles by recycling poly(lactic acid) (PLA) waste from coffee machine pods, incorporating carbon black (CB) as a conductive filler for electroanalytical sensing applications.

In parallel, there is significant potential to explore alternative materials derived from agro-industrial waste to produce FFF filament composites [17–19], further enhancing the sustainability of FFF processes. Natural waste materials, such as those from agriculture, present promising alternatives for creating sustainable, printable materials for AM [20, 21].

One such material is biochar, a carbon-rich substance derived from the pyrolysis of biomass, which has attracted considerable interest due to its environmental benefits [22]. Originally used for applications such as soil remediation, carbon sequestration, water purification, and air filtration, biochar is now being considered as a reinforcing filler in composite materials [20]. Its high carbon content, large surface area, and stable composition make it an ideal candidate for such applications [15, 23]. Several studies have integrated biochar into natural polymers, assessing its impact on the mechanical properties of the resulting composites sources [19, 24–26]. Additionally, Silva et al. [20] utilized adsorption properties of biochar to develop composite materials for removing contaminants from water. However, to date, no research has explored the use of biochar-based polymer composites for 3D-printed electrodes, which presents a clear gap in the field.

Among various biomass precursors used for biochar production, coconut shell stands out due to its unique physicochemical characteristics. As an agricultural waste widely available in tropical regions, coconut shell offers a sustainable and economically viable source of carbon-rich material [27]. Its inherently dense and lignocellulosic structure yields biochar with high fixed carbon content, low ash, and well-developed porosity after pyrolysis [27, 28].

These features are particularly advantageous for applications requiring enhanced surface area, structural stability, and electrical conductivity, such as in energy storage devices, catalysis, and environmental remediation. Compared to other biochar sources, coconut shell–derived biochar exhibits superior conductivity and a more stable microstructure, making it a promising candidate for advanced material development.

From an electrochemical perspective, the properties of biochar, such as its large surface area, porosity, and high cation exchange capacity, are closely linked to its ability to pre-concentrate analytes and interact with other species. As a result, biochar has been widely employed as an electrode modifier for the electrochemical detection of various compounds. Electrodes modified with biochar can be designed in various configurations, leveraging biochar's capacity for direct analyte preconcentration (via sorption) followed by subsequent detection [15].

Herein, we propose a development of a novel FFF–filament composite incorporating biochar derived from coconut agro-waste, carbon black (CB), PLA as the polymer matrix, and castor oil as a bioplasticizer. The composite was synthesized via a thermal mixing method, which avoids the use of hazardous solvents commonly required in other fabrication techniques. After optimizing the composite material, its electrochemical properties were thoroughly characterized, demonstrating its potential for sensor applications. Specifically, we successfully employed the composite as an electrochemical sensor for the detection of carbendazim in environmental water samples.

This work represents the first use of a biochar-based composite filament in the development of electroanalytical sensing platforms, providing a novel, sustainable approach for 3D-printed sensors. Moreover, the proposed method offers significant advantages in terms of cost-effectiveness, scalability, and environmental sustainability, marking an important step toward more sustainable additive manufacturing practices.

Materials and methods

More information regarding this topic is available in Supporting Information.

Production of additively manufactured filament composite and working electrode

Figure 1 presents a schematic representation of the steps involved in the production of the FFF–filament composite and the printing of additively manufactured working electrodes. This filament was produced by a thermal mixing–based method and is composed of 20 wt.% CB, 10 wt.% biochar, 10 wt.% castor oil, and 60 wt.% PLA. The mixture was prepared in a glass container (Fig. 1A) at 200 °C under stirring until the formation of a homogeneous material (Fig. 1B). We attempted to incorporate a higher concentration of biochar; however, the generated composite could not be extruded. The resulting composite was allowed to cool to room temperature before being crushed in an FTR1 grinder (Filmaq 3D, Curitiba, Brazil) (Fig. 1C). Subsequently, the material was processed using a single-screw extruder (Filmaq 3D, Curitiba, Brazil) at 220 °C (with a 1.75-mm-inner-diameter nozzle) and an extrusion speed of 30 mm s^{-1} (Fig. 1D). The working electrodes were then printed using a FlashForge Dreamer NX printer (São José dos Campos, Brazil) equipped with a 0.8-mm nozzle at 220 °C and a bed temperature of 90 °C. The printing parameters were set with

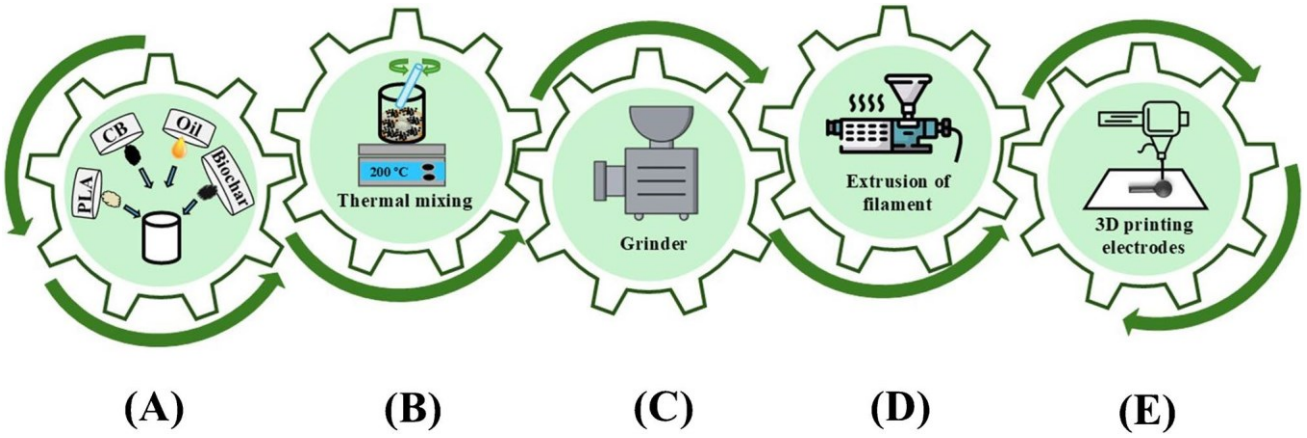

Fig. 1 A representative scheme to produce FFF-filament based on CB, PLA, biochar, and castor oil. **(A)** Initial mixing of the three materials; **(B)** thermal mixing (200 °C); **(C)** crushing the material using an FTR1 grinder; **(D)** filament production using an extruder; **(E)** additively manufactured electrode construction

a layer thickness of 0.15 mm, two perimeters in a horizontal orientation with 100% infill density, and a constant perimeter printing speed of 60 mm s^{-1}, similarly described by Siqueira et al. [29] who developed 3D-printed electrodes made from commercial conductive filament. Figure S1 displays real images of the materials obtained from both processes described above.

Results and discussion

Morphological and spectroscopic characterization

The commercial biochar used in this work was derived from coconut shell. According to the literature, this biomass is primarily composed of cellulose (26.6 wt.%), hemicellulose (21 wt.%), lignin (29.4 wt.%), pentosans (27.7 wt.%), uronic anhydrides (3.5 wt.%), and ash (0.6 wt.%) [19]. Previous research has demonstrated that this biomass has a high carbon content, making it an efficient feedstock for biochar production. In fact, coconut shell–derived biochar has been widely used as an adsorbent due to its high porosity and large surface area [23, 30, 31]. Thus, the morphology of biochar was initially evaluated by SEM imaging (Fig. S2). As can be seen, the biochar from coconut shell contains a diverse range of irregularly shaped particles and chunks, which is consistent with observations reported in the literature [19, 26]. Moreover, EDS analysis displayed the presence of carbon, oxygen, calcium, iron, potassium, silicon, and aluminum (Fig. S3). These results are consistent with previous studies on biochar derived from this biomass [19, 32]. As expected, the pyrolysis process resulted in a significant concentration of carbon in the biochar. The presence of other elements (K, Fe, Ca, and Al) was also detected, reflecting the composition of the coconut shell biomass [33].

The production of additive manufacturing FFF–filament, composed of biochar (10 wt.%), PLA (60 wt.%), castor oil (10 wt.%), and CB particles (20 wt.%), was carried out following the methodology proposed by the research group [34]. This approach involves a single thermal mixing step, which effectively eliminates the use of toxic organic solvents, offering a significant advantage over other production methods [35]. As shown in Fig. 2A, the resulting filament exhibited excellent flexibility at room temperature. In addition, the resistance along the connection length of the laboratory-made filament was measured using a multimeter, exhibiting a resistance of 875 ± 22 Ω over a 10-cm length. This value is highly consistent with other laboratory-made filaments reported in the literature [14, 36]. Notably, this value shows a significant improvement compared to the resistance of commercial conductive filaments (composed of CB and PLA particles), which typically range from 2.0 to 3.5 kΩ [37]. This improvement in resistance is likely attributed to the higher carbon loading in the filament, particularly due to the presence of biochar, which enhances its conductivity.

Subsequently, the thermal properties of the filament composite, composed of biochar, PLA, CB, and castor oil, were evaluated using thermogravimetric analysis (TGA; Fig. 2B, Table S1). To assess the effect of biochar on the filament properties, additional characterizations were performed on a laboratory-made filament containing only CB, PLA, and castor oil for comparison. The thermal properties of each individual component were also evaluated separately. In the biochar, the initial onset of degradation temperature, observed at around 67 °C, is attributed to the loss of adsorbed water and the release of a small amount of simpler volatile components. The second degradation step at 264 °C is related

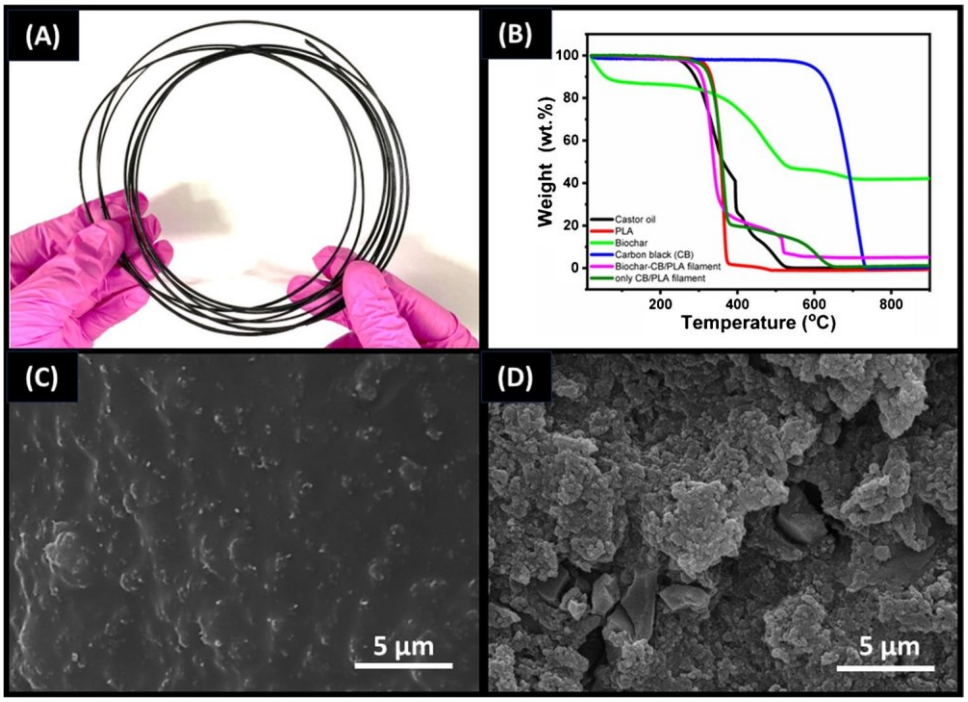

Fig. 2 **(A)** Images of the biochar-CB/PLA filament illustrating its flexibility; **(B)** thermogravimetric analysis (TGA) of castor oil (black line), biochar (green line), CB powder (blue line), PLA pellets (red line), biochar-CB/PLA (magenta line), and only-CB/PLA (olive line) filaments. SEM images obtained **(C)** before and **(D)** after electrochemical treatment procedure on biochar-CB/PLA electrode surface

to hemicellulose decomposition [38]. At approximately 527 °C, the degradation of lignin from the biomass occurs. Finally, a mass loss was observed at 667 °C, attributed to the degradation of inorganic compounds. These results agreed with previous research exploring the thermal stability of biochar [32, 38]. Castor oil exhibited an onset temperature of 215 °C, as previously reported [11]. A single thermal event was observed for CB, occurring between 546 and 692 °C, which corresponds to its thermal decomposition. For the PLA polymer, two distinct thermal events can be identified. The first process, occurring at around 274 °C, corresponds to the decomposition of PLA into carbon dioxide, carbon monoxide, and cyclic oligomers down to the monomeric unit. The second event, observed at approximately 419 °C, is associated with the further decomposition of the remaining material [39].

The TGA revealed that the onset temperature for CB/PLA matrix system was lower compared to that of virgin PLA. This effect is more pronounced in the biochar-infused PLA matrix system (biochar-CB/PLA). This behavior was also observed by Terzioglu and co-workers [40] in polyvinyl alcohol (PVA)–biochar composites, where the presence of biochar in the PLA matrix accelerated the breakdown of the polymer, leading to earlier degradation. Additionally, Arrigo et al. [41] demonstrated that the presence of metal impurities in biochar (as observed by EDS analysis) has a detrimental effect on the thermal stability of PLA, further contributing to the observed decrease in thermal resistance. From the stabilization of the TGA curve after the degradation of PLA, CB particles, and castor oil, the biochar content of the filament was calculated to be 7.1 ± 1.9 wt.%. This difference probably is associated with mass loss during the filament production process.

Figure S4A displays real images of additively manufactured lollipop-shaped electrodes, indicating excellent printability without the need for additional extrusion rates to achieve high-quality prints. To better understand the impact of biochar on the system, it is important to compare the custom-made filament with a filament containing only the same CB filler. As previously reported, the additively manufactured electrodes exhibited poor electrochemical activity due to the insulating nature of the polymer material [42]. As a result, both electrodes were subjected to (electro)chemical activation in a basic medium [43]. Although some studies reported improvements in the electrochemical activity after the treatment, no significant changes were observed following the activation procedures [44, 45]. In fact, no differences were observed in the Raman spectra for both electrode surfaces after the treatment (data not shown). Figure S4B displays Raman spectra obtained for both electrode surfaces. The presence of the D (1350 cm^{-1}), G (1609 cm^{-1}), and 2D (2813 cm^{-1}) bands was observed, as expected for carbonaceous materials [44]. The D band originates from structural defects and the presence of sp^2 carbon bonds. The G peak corresponds to the vibrational mode of graphitic carbon in the sp^2 plane while the 2D peak is associated with the number of graphitic layers. However, the intensity of the 2D band observed for biochar-CB/PLA electrode is lower than that of the CB/PLA filament in the Raman spectra, which

can be explained by the disruption of the regular layered structure of conductive material, as reported by other authors [46, 47].

Next, the morphology of the additively manufactured electrodes was analyzed using SEM images. As observed in Fig. 2 C, the non-treated biochar-CB/PLA electrode revealed a non-uniform texture, with irregular structures (flakes) embedded within the PLA matrix. For the activated biochar-CB/PLA electrode (Fig. 2D), partial removal of the PLA material through a saponification reaction on the surface resulted in a noticeable increase in porosity. This enhancement facilitated greater access for electrochemically active species to the conductive carbon. Additionally, the SEM images revealed irregularly shaped particles and chunks, similar to those observed in the biochar SEM images (Fig. S2), indicating the successful incorporation of biochar into the FFF–filament composite.

The SEM image of the CB/PLA composite (Fig. S5) reveals a predominantly smooth PLA surface, with nanoparticles being barely visible. Upon activation, a significant portion of the PLA coating is removed, exposing a greater amount of the CB filler. Notably, no distinctly shaped particles or chunks are observed, confirming the absence of biochar, as expected. EDS analysis of the biochar-CB/PLA electrodes (Fig. S6) detected the presence of oxygen, carbon, iron, and calcium, whereas the CB/PLA electrodes exhibited only carbon and oxygen (Fig. S7). These results are consistent with previous EDS studies on biochar, which identified trace metals such as calcium and iron.

Electrochemical characterization

The initial electrochemical characterization was conducted using inner $[Fe(CN)_6]^{3-/4-}$ and outer $[Ru(NH_3)_6]^{2+/3+}$ redox probes in a 0.1 mol L^{-1} KCl solution by CV measurements, all at a concentration of 1.0 mmol L^{-1} and 3D-printed electrodes in a simple lollipop-shaped design (see Fig. S4A). The analysis was performed on both biochar-CB/PLA and CB/PLA electrodes, with a pre-concentration time of 1 min to verify the adsorption process from biochar. The results summarized in Table S1 indicate that both electrodes exhibited a significant improvement in the electrochemical response of the two evaluated compounds. These findings were further corroborated by SEM images of both electrodes, which revealed increased exposure of conductive fillers, supporting the enhanced performance. It is also possible to observe that the voltammetric profile (current intensity and peak-to-peak separation) for the biochar-CB/PLA electrode is better than that of the CB/PLA electrode. These enhancements can be attributed to multiple mechanisms, particularly partitioning or physical adsorption, as well as electrostatic and π–π interactions [38], which play a significant role in facilitating improved electrochemical behavior.

Moreover, the *Rct* values obtained from EIS measurements (Fig. 3C) agreed with the results described above, with the treated-biochar-CB/PLA electrodes showing a significantly lower charge transfer resistance (*Rct* = 1.01 ± 0.05 and 9.11 ± 0.03 kΩ for biochar-CB/PLA and CB/PLA electrodes, respectively) compared to the treated CB/PLA electrode. A summary of these results on the electrochemical performance of both evaluated 3D-printed electrodes is described in Table S1, highlighting the peak-to-peak separation (ΔEp) and anodic current intensity (Ip_a) for outer- and inner-sphere redox couples, as well as the *Rct* values from the Nyquist plot.

It is worth highlighting that various conductive fillers have been previously incorporated into PLA matrices, including graphite [48, 49], multi-walled carbon nanotubes (MWCNTs) [50], CB [51], graphene [52], carbon nanofibers [53], and boron-doped nanodiamond foil [54]. However, our proposed filament composite presented similar electrochemical response for ideal redox probes compared to other conductive materials with higher cost. For instance, Crapnell et al. [50] developed a PLA-based composite containing MWCNTs and CB, which exhibited a peak-to-peak separation of 111 mV at a scan rate of 25 mV s^{-1} using $[Ru(NH_3)_6]^{2+/3+}$ as the redox probe. In contrast, our proposed electrodes achieved a narrower peak-to-peak separation of 89 ± 3 mV at 50 mV s^{-1}, highlighting their competitive performance.

Electrochemical determination of carbendazim

To evaluate the ability of biochar (with negative charges on its surface) to preconcentrate carbendazim (CBZ), which becomes protonated in acidic solutions, forming positively charged species, on the electrode surface, the electrochemical behavior of 10 µmol L^{-1} CBZ was investigated using DPV measurements. These measurements were conducted with the two electrodes under evaluation, specifically the CB/PLA and biochar-CB/PLA, in a 0.1-mol L^{-1} acetate buffer solution (pH 4.0). Before analysis, both electrodes were subjected to the same preconcentration process without applied potential and under constant stirring for 2 min, as previously described by Sant'anna et al. [38], Fig. 4A. As observed, a peak at around + 0.92 V (vs. $Ag|AgCl|KCl_{(sat.)}$) was detected for CBZ oxidation at both evaluated electrodes. Moreover, for the biochar-CB/PLA electrode, the oxidation peak current increase from 0.62 ± 0.01 µA to 1.21 ± 0.07 µA (~ twofold higher). This result is consistent with previous electrochemical characterizations described above, including the *Rct* value and voltammetric profiles for evaluated redox probes. The enhancement in the faradaic current can be attributed to the functional groups (bearing negative

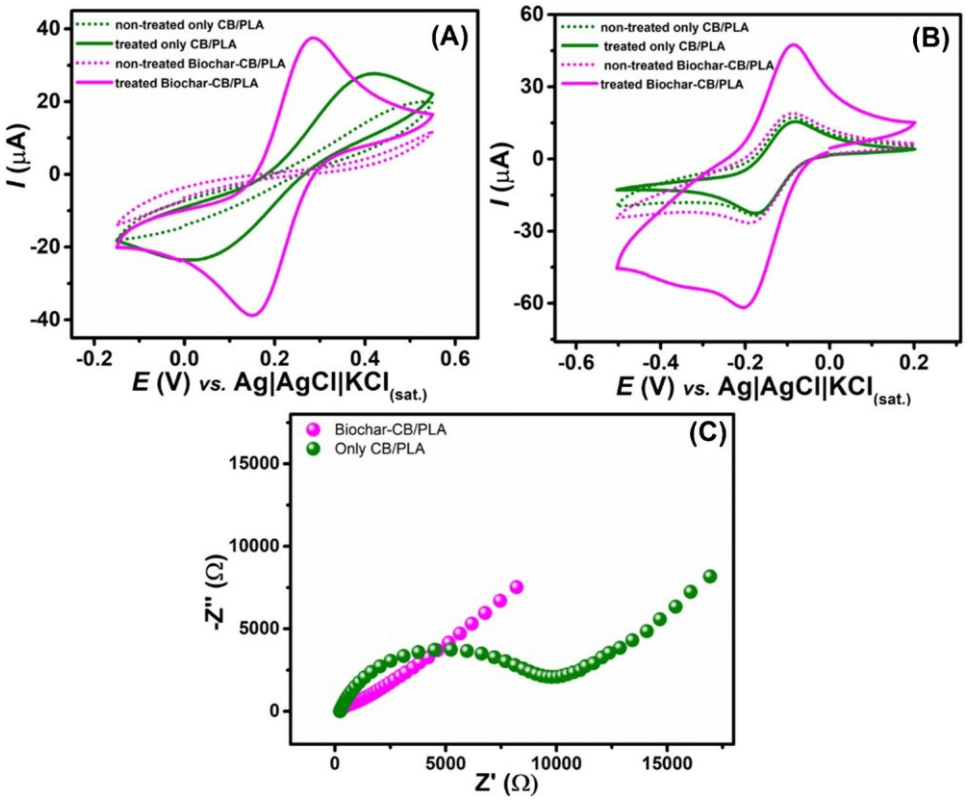

Fig. 3 Cyclic voltammograms recorded in the presence of **(A)** 1.0 mmol L^{-1} $[Fe(CN)_6]^{3-/4-}$ and **(B)** 1.0 mmol L^{-1} $[Ru(NH_3)_6]^{2+/3+}$ at the biochar-CB/PLA (magenta line) and CB/PLA (olive line) electrodes, using a 0.1 mol L^{-1} KCl solution as the supporting electrolyte. The dashed and solid lines represent the measurements before and after electrochemical treatment of the electrode surfaces, respectively. CV conditions: scan rate = 50 mV s^{-1}; step potential = 5 mV. **(C)** EIS Nyquist plots recorded in the presence of 1.0 mmol L^{-1} $[Fe(CN)_6]^{3-/4-}$ at an applied potential of + 0.15 V (vs. $Ag|AgCl|KCl_{(sat.)}$) for both the biochar-CB/PLA (magenta line) and CB/PLA (olive line) electrodes after electrochemical treatment

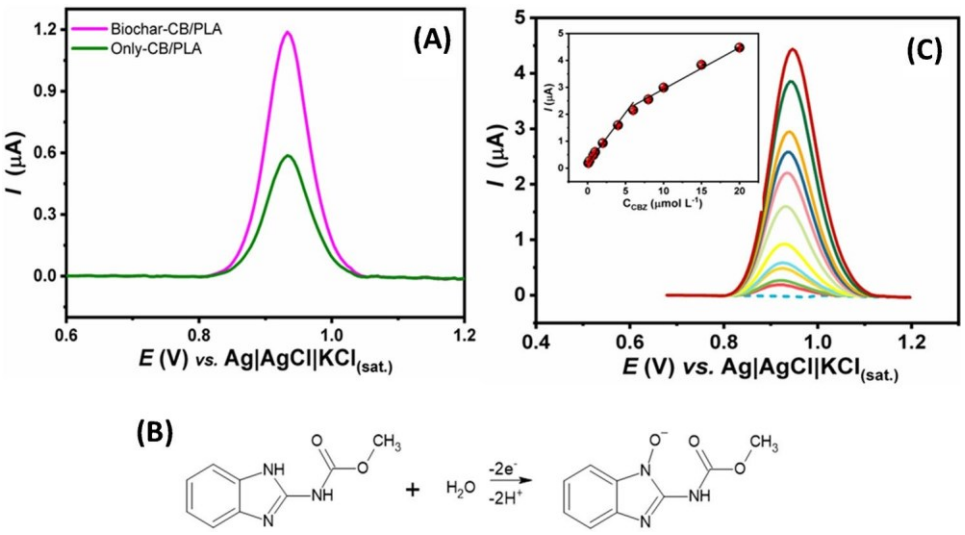

Fig. 4 **(A)** Baseline-corrected DPV scans recorded in the presence of 10 μmol L^{-1} CBZ in 0.1 mol L^{-1} acetate buffer (pH = 4.0) as supporting electrolyte, using the CB/PLA and biochar-CB/PLA electrodes, both electrochemically treated in a basic medium. DPV conditions: amplitude = 50 mV; step potential = 5 mV. **(B)** Proposed electrochemical reaction for CBZ. **(C)** Baseline-corrected DPV responses for increasing concentrations of CBZ (0.1 to 20.0 μmol L^{-1}) using biochar-CB/PLA electrode along with respective calibration plot. All experiments were performed using BR buffer (pH = 4.0) as supporting electrolyte. DPV conditions: amplitude = 70 mV; ΔE_p = 6 mV; modulation time = 30 ms

charges) present in the biochar, which facilitate more efficient interactions with CBZ (protonated and positively charged) and the electrode surface. Several mechanisms may contribute to these interactions, including partitioning, physical adsorption, electrostatic interactions, and π–π interactions. Typically, the observed improvement results from

a combination of these mechanisms working synergistically [55, 56].

To achieve optimal performance for detecting CBZ, the influence of pH on the electrochemical response of 10.0 µmol L^{-1} CBZ was assessed using BR buffer solutions (pH = 2.0–10.0) at the biochar-CB/PLA electrode, as shown in Fig. S8. As observed, there was a shift to less positive values with increasing pH. Moreover, a pH-dependent oxidation peak (55 mV pH^{-1}) was achieved in the evaluated pH range, indicating an equal number of electrons and protons involved in the reaction [38, 57–59]. The best electrochemical response was achieved at pH 4.0, and this medium was selected as the supporting electrolyte for further studies. This behavior can be attributed to the protonation of CBZ molecule (pK_a = 4.6) in this medium, as biochar presents negative charges on its surface [60], facilitating the interaction between CBZ and the electrode surface [57, 61].

Afterwards, CV scan rate studies (1–150 mV s^{-1}) were also performed in the presence of 1 mmol L^{-1} CBZ in BR buffer (pH = 4.0), as can be seen in Fig. S9. The experimental result (Ip vs. $v^{1/2}$) indicated that diffusional process takes place in the electrochemical detection of CBZ. In addition, this was also checked with the plot of log Ip versus log scan rate, in which a slope close to 0.5 was obtained, indicating a diffusion-controlled process [62]. In addition, using the following equation [63]:

$$\frac{E_p}{\log v} = \frac{30\,\text{mV}}{an}$$

where E_p is the peak oxidation position, v is the scan rate, α is the coefficient of electron transfer, and n is the number of electrons involved in the reaction, thus, assuming α as 0.5 for organic compounds with irreversible process [63]. The number of electrons estimated is 2.14, or approximately 2. Figure 4B displays the proposed reaction previously described in the literature [59].

Considering the adsorption effect of CBZ on the electrode surface, we investigated the influence of adsorption time (10 to 100 s) and stirring speed (200 to 1334 rpm) on the electrochemical response of 10 µmol L^{-1} CBZ using DPV scans (Figs. S10 and S11, respectively). As observed, the peak current increased with both parameters, suggesting the accumulation of CBZ on the electrode surface. Furthermore, the response current reached its maximum after 60 s of adsorption time and a stirring speed of 750 rpm. These results indicate that the active sites on the biochar-CB/PLA surface were probably saturated under these conditions. Therefore, these parameters were selected for subsequent experiments.

In the next step, DPV parameters were systematically optimized, considering their effect on the voltammetric current intensity. Specifically, the pulse amplitude (a) was studied in a range from 10 to 100 mV, and the step potential (ΔE_s) was varied from 1 to 8 mV. These parameters were evaluated by analyzing the peak position, current intensity, and peak width at half height, using a 10-µmol L^{-1} CBZ solution in 0.12 mol L^{-1} BR buffer (pH = 4.0), as shown in Figs. S12 and S13. As can be seen, the optimal performance was achieved under the following conditions: a = 70 mV; ΔE_s = 6 mV.

Under optimized conditions, a calibration curve was constructed for biochar-CB/PLA electrodes. Figure 4C shows DPV scans recorded at biochar-CB/PLA and respective calibration plot. Additionally, Table 1 summarizes the analytical parameters including the linear range, limit of detection (LOD), and slope (sensitivity), using the biochar-CB/PLA electrode. As observed, two linear ranges were achieved (0.1–5.0 and 5.0 to 20.0 µmol L^{-1} CBZ), with a high coefficient of determination ($R^2 > 0.995$). The LOD was determined according to IUPAC guidelines ($3.3\sigma/s$), where σ is the standard deviation of successive measurements of the blank signal and s is the analytical sensitivity (slope) of the analytical curve obtained through first linear range. Notably, the LOD value of 0.01 µmol L^{-1} obtained with the proposed sensor is appropriate for detecting CBZ in environmental samples. For example, Chen et al. [64] analyzed paddy water samples from China and reported a CBZ concentration of 0.58 µmol L^{-1}, while Derbalah and co-workers [65] evaluated samples from Kurose River in Japan and found 4.23 µg L^{-1} (0.02 µmol L^{-1}) CBZ.

The intra-electrode precision of the proposed method was also studied with successive DPV measurements (n = 10) recorded at two CBZ concentrations (0.25 and 3.0 µmol L^{-1}) in BR buffer (pH = 4.0), as shown in Fig. S14. The relative standard deviation (RSD) value attested good precision for this method using the biochar-CB/PLA electrodes (RSD < 4.9%).

The inter-electrode precision was also assessed with the electrochemical response of 6.0 µmol L^{-1} CBZ in BR buffer solution, using different electrodes (n = 3), Fig. S15. The obtained RSD value (< 5%) showed satisfactory inter-electrode precision.

Regarding stability, electrodes 3D-printed 6 months ago did not exhibit the same electrochemical response (no

Table 1 Analytical parameters obtained for CBZ detection at biochar-CB/PLA electrode

Analytical parameters	Carbendazim
Linear range, µmol L^{-1}	0.1–5.0 to 5.0–20.0
R^2	0.997/0.995
Intercept, µA	0.179 ± 0.007/1.396 ± 0.0951
Slope, µA L $µmol^{-1}$	0.376 ± 0.008/0.154 ± 0.005
LOD, µmol L^{-1}	0.01
RSD (n = 10), %	4.9*/3.2**

For *0.25 and **3.0 µmol L^{-1} CBZ in BR buffer (pH =4.0)

response was observed). Nevertheless, it is well known that 3D-printed electrodes tend to lose their electrochemical performance over time, as demonstrated by Kalinke et al. [66], likely due to the high water absorption of the polymeric matrix [67].

Next, we compared the analytical parameters obtained using the biochar-CB/PLA electrodes with those of other electrochemical methods reported in the literature (Table S2). More information about other electrochemical methods described in the literature is reviewed by Crapnell et al. [59]. As observed, our proposed method demonstrated comparable or superior analytical performance to most of the studies listed in Table S2, even when using conventional electrodes such as boron-doped diamond [68] or involving complex modified electrodes [69, 70]. While some studies reported a lower LOD for CBZ detection, these methods often required labor-intensive and costly procedures. Other research employed additive-manufactured electrodes based on CB-PLA [71] and graphite-PLA (Gpt-PLA) composites [72]; however, our approach still demonstrated superior analytical performance. Furthermore, both studies [71, 72] relied on toxic organic solvents to fabricate FFF filaments (non-eco-friendly), whereas our study avoided the use of any hazardous materials and generated minimal waste (often zero).

By developing a PLA-biochar filament-based electrode, we provide a more straightforward, accessible, and sustainable method for sensor fabrication compared to the more complex electrode modifications in existing literature, including other electrodes modified with biochar-based materials [73]. This approach offers several advantages, including environmental benefits, cost-effectiveness, and ease of use. Additionally, the inclusion of agro-industrial waste as a biochar precursor enhances the adsorption of carbendazim (CBZ) on the electrode surface, thereby improving its electrochemical performance.

The FFF 3D-printing technique, which is highly cost-effective (with electrode production costing only $0.04), makes this method even more attractive for large-scale applications. Biochar, an eco-friendly and sustainable material, has proven effective in various electrochemical sensing applications, particularly in detecting cationic compounds, further emphasizing the practicality and innovation of our approach [22, 55].

Real sample analysis

To show the potential applicability of the electrochemical sensing platform to determine CBZ in various samples, we analyzed water (tap, drinking, and lake) and lemon juice samples spiked with CBZ at two concentrations. The spiked samples were then analyzed using the standard addition method (see Table 2 and Fig. S16). As observed, before spiking, no analytical signals (< LOD) were detected near the CBZ peak position in any of the samples. Following the analysis of the spiked samples, the obtained recovery values (90–115%) demonstrated the accuracy of the proposed method, which was free from interference from both sample matrices. The recovery values obtained in these analyses are in accordance with the acceptable range established by the National Institute of Metrology, Quality and Technology (Inmetro) in Brazil, which considers values between 80 and 120% acceptable for the mass fraction of this type of sample [74].

Table 2 Results (mean ±SD) for the determination of CBZ in environmental and food samples using the proposed DPV method and biochar-CB/PLA working electrodes

Samples	Added (μmol L^{-1})	Found (μmol L^{-1})	Recovery (%)
Tap water	0.00	< LOD	–
	0.20	0.18 ±0.01	90 ±5
	0.30	0.28 ±0.02	93 ±7
Lake water	0.00	< LOD	–
	0.20	0.21 ±0.01	105 ±5
	0.30	0.31 ±0.02	103 ±7
Drinking water	0.00	< LOD	–
	0.20	0.18 ±0.01	90 ±5
	0.30	0.31 ±0.03	103 ±10
Lemon juice[a]	0.00	< LOD	–
	0.10	0.09 ±0.01	90 ±10
	0.20	0.23 ±0.02	115 ±10

[a]These analyses were carried out after tenfold dilution in the supporting electrolyte

Interfering species

Some compounds, such as glucose (GLU), paracetamol (PAR), caffeine (CAF), ciprofloxacin (CIP), and sodium chloride, can be found in food or environmental samples and may interfere with the electrochemical response of CBZ on biochar-CB/PLA electrode. For this reason, 2.5 μmol L^{-1} CBZ was mixed with interfering species at different ratios (1:1 and 1:2), as shown in Fig. S17. As can be observed, GLU and NaCl did not significantly interfere with the CBZ current signal (< 10%). On the other hand, although CIP and CAF did not exhibit an oxidation peak in the same potential region, they significantly reduced the CBZ response. However, these influences can be minimized by using the standard addition method.

Conclusions

Herein, a simple route was used to produce flexible FFF–filaments based on biochar, CB particles, PLA, and castor oil as a plasticizer. Unlike commonly used methods for the construction of conductive filaments, this approach does not require laborious, costly, and hazardous solvents to form the filament composite. Moreover, biochar-CB/PLA electrode demonstrated superior electrochemical performance compared to the CB/PLA electrode (as observed through cyclic voltammetric measurements for redox couples), attributed to the high specific surface area of biochar. From the morphological characterizations, the presence of biochar was observed, confirming the successful incorporation of this material into PLA matrix. We demonstrated the potential of biochar-CB/PLA-based sensors for detecting CBZ in environmental and food samples. The sensors benefit from the high carbon content and large specific surface area of biochar, which enhance the electrochemical activity of the electrode.

Our proposed method can enhance the sustainability of 3D-printing technology, offering a cost-effective and easy-to-use strategy for the large-scale fabrication of FFF–filament composite based on agro-residue waste. The produced filament can potentially be applied for detecting different analytes, such as metals or organic compounds. Moreover, the new material will be further explored in the near future as it could offer outstanding solutions and new opportunities in the (bio)sensor field and the construction of various electronic devices such as supercapacitors, batteries, and others.

Acknowledgements The facilities provided by RELAM-UFU multiuser laboratory are acknowledged.

Funding The authors are grateful for the financial support provided by CAPES (code 001), CNPq (408462/2022–1, 308392/2022–1, 405620/2021–7, 405620/2021–7, 401977/2023–4, and 315838/2021–3), and FAPEMIG (RED-00120–23, APQ-02391-22 (RELAM-UFU facilities) and APQ-02067–23), INCT of Bioanalytics (CNPq/INCT 465389/2014–7), and INCT-SP (CNPq 406958/2022–0).

Data Availability We provided a supplementary file with all experimental data. If additional information is necessary, it will made available upon request.

Declarations

Competing interests The authors declare no competing interests.

References

1. Attaran M (2017) The rise of 3-D printing: the advantages of additive manufacturing over traditional manufacturing. Bus Horiz 60:677–688. https://doi.org/10.1016/j.bushor.2017.05.011
2. Ikram H, Al Rashid A, Koç M (2022) Additive manufacturing of smart polymeric composites: literature review and future perspectives. Polym Compos 43:6355–6380. https://doi.org/10.1002/pc.26948
3. Paris H, Mokhtarian H, Coatanéa E et al (2016) Comparative environmental impacts of additive and subtractive manufacturing technologies. CIRP Ann 65:29–32. https://doi.org/10.1016/j.cirp.2016.04.036
4. Wu H, Mehrabi H, Karagiannidis P, Naveed N (2022) Additive manufacturing of recycled plastics: strategies towards a more sustainable future. J Clean Prod 335:130236. https://doi.org/10.1016/j.jclepro.2021.130236
5. Tadi SP, Maddula SS, Mamilla RS (2024) Sustainability aspects of composite filament fabrication for 3D printing applications. Renew Sustain Energy Rev 189:113961. https://doi.org/10.1016/j.rser.2023.113961
6. Davis JT, Jayathilake BS, Chandrasekaran S et al (2024) 3D printed optimized electrodes for electrochemical flow reactors. Sci Rep 14:22662. https://doi.org/10.1038/s41598-024-71765-w
7. Ambaye AD, Kefeni KK, Mishra SB et al (2021) Recent developments in nanotechnology-based printing electrode systems for electrochemical sensors. Talanta 225:121951. https://doi.org/10.1016/j.talanta.2020.121951
8. Rahim TNAT, Abdullah AM, Md Akil H (2019) Recent developments in fused deposition modeling-based 3D printing of polymers and their composites. Polym Rev 59:589–624. https://doi.org/10.1080/15583724.2019.1597883
9. Kumar S, Singh H, Singh I et al (2024) A comprehensive review of FDM printing in sensor applications: advancements and future perspectives. J Manuf Process 113:152–170. https://doi.org/10.1016/j.jmapro.2024.01.030
10. Camargo JR, Crapnell RD, Bernalte E et al (2024) Conductive recycled PETg additive manufacturing filament for sterilisable electroanalytical healthcare sensors. Appl Mater Today 39:102285. https://doi.org/10.1016/j.apmt.2024.102285
11. Crapnell RD, Arantes IVS, Whittingham MJ et al (2023) Utilising bio-based plasticiser castor oil and recycled PLA for the production of conductive additive manufacturing feedstock and detection of bisphenol A. Green Chem 25:5591–5600. https://doi.org/10.1039/D3GC01700A
12. Peeters B, Kiratli N, Semeijn J (2019) A barrier analysis for distributed recycling of 3D printing waste: taking the maker movement perspective. J Clean Prod 241:118313. https://doi.org/10.1016/j.jclepro.2019.118313
13. Fico D, Rizzo D, De Carolis V et al (2022) Sustainable polymer composites manufacturing through 3D printing technologies by using recycled polymer and filler. Polymers (Basel) 14:3756. https://doi.org/10.3390/polym14183756
14. Crapnell RD, Sigley E, Williams RJ et al (2023) Circular economy electrochemistry: recycling old mixed material additively manufactured sensors into new electroanalytical sensing platforms. ACS Sustain Chem Eng 11:9183–9193. https://doi.org/10.1021/acssuschemeng.3c02052
15. Kalinke C, de Oliveira PR, Bonacin JA et al (2021) State-of-the-art and perspectives in the use of biochar for electrochemical and electroanalytical applications. Green Chem 23:5272–5301. https://doi.org/10.1039/D1GC00843A
16. Sigley E, Kalinke C, Crapnell RD et al (2023) Circular economy electrochemistry: creating additive manufacturing feedstocks for caffeine detection from post-industrial coffee pod waste. ACS

Sustain Chem Eng 11:2978–2988. https://doi.org/10.1021/acssuschemeng.2c06514
17. Ganguly A, Shankar S, Das A et al (2022) Natural fibre reinforced composites: a review based on additive manufacturing routes and biodegradability perspective. Mater Today Proc 62:131–135. https://doi.org/10.1016/j.matpr.2022.02.607
18. Khalid MY, Al Rashid A, Arif ZU et al (2021) Natural fiber reinforced composites: sustainable materials for emerging applications. Results in Engineering 11:100263. https://doi.org/10.1016/j.rineng.2021.100263
19. Umerah CO, Kodali D, Head S et al (2020) Synthesis of carbon from waste coconutshell and their application as filler in bioplast polymer filaments for 3D printing. Compos B Eng 202:108428. https://doi.org/10.1016/j.compositesb.2020.108428
20. Silva EC, Soares VR, Nörnberg AB, Fajardo AR (2023) Recyclable 3D-printed composite hydrogel containing rice husk biochar for organic contaminants adsorption in tap water. ACS Appl Polym Mater 5:8415–8429. https://doi.org/10.1021/acsapm.3c01534
21. Kalinke C, Crapnell RD, de Oliveira PR et al (2024) How to improve sustainability in fused filament fabrication (3D Printing) research? Global Challenges 8:2300408. https://doi.org/10.1002/gch2.202300408
22. Rizwan M, Ali S, Qayyum MF et al (2016) Mechanisms of biochar-mediated alleviation of toxicity of trace elements in plants: a critical review. Environ Sci Pollut Res 23:2230–2248. https://doi.org/10.1007/s11356-015-5697-7
23. Rajapaksha AU, Chen SS, Tsang DCW et al (2016) Engineered/designer biochar for contaminant removal/immobilization from soil and water: potential and implication of biochar modification. Chemosphere 148:276–291. https://doi.org/10.1016/j.chemosphere.2016.01.043
24. Shao Y, Wang J, Wu H et al (2024) Shape stability control of a 3D-printed clay/biochar-based monolith to support Fe catalyst for continuous levofloxacin degradation with low metal leaching. Colloids Surf A Physicochem Eng Asp 680:132664. https://doi.org/10.1016/j.colsurfa.2023.132664
25. Anerao P, Kulkarni A, Munde Y et al (2023) Biochar reinforced PLA composite for fused deposition modelling (FDM): a parametric study on mechanical performance. Composites Part C: Open Access 12:100406. https://doi.org/10.1016/j.jcomc.2023.100406
26. Petousis M, Maravelakis E, Kalderis D et al (2024) Biochar for sustainable additive manufacturing: thermal, mechanical, electrical, and rheological responses of polypropylene-biochar composites. Biomass Bioenergy 186:107272. https://doi.org/10.1016/j.biombioe.2024.107272
27. Mas'udah KW, Nugraha IMA, Abidin S et al (2016) Solution of reduced graphene oxide synthesized from coconut shells and its optical properties. AIP Conf Proc 1725:020045. https://doi.org/10.1063/1.4945499
28. Kishore Chowdari G, Krishna Prasad DVV, Devireddy SBR (2020) Physical and thermal behaviour of areca and coconut shell powder reinforced epoxy composites. Mater Today Proc 26:1402–1405. https://doi.org/10.1016/j.matpr.2020.02.282
29. Siqueira GP, Rocha RG, Nascimento AB et al (2024) Portable atmospheric air plasma jet pen for the surface treatment of three-dimensionally (3D)-printed electrodes. Anal Chem 96:15852–15858. https://doi.org/10.1021/acs.analchem.4c02785
30. Paranavithana GN, Kawamoto K, Inoue Y et al (2016) Adsorption of Cd2+ and Pb2+ onto coconut shell biochar and biochar-mixed soil. Environ Earth Sci 75:484. https://doi.org/10.1007/s12665-015-5167-z
31. Liu H, Xu F, Xie Y et al (2018) Effect of modified coconut shell biochar on availability of heavy metals and biochemical characteristics of soil in multiple heavy metals contaminated soil. Sci Total Environ 645:702–709. https://doi.org/10.1016/j.scitotenv.2018.07.115
32. Arandara KP, Paranavithana GN, Priyadarshana ST et al (2024) Investigating coconut shell biochar as a sustainable solution for removing iron residues in recycled concrete aggregates. Clean Technol Environ Policy. https://doi.org/10.1007/s10098-024-03029-0
33. Liyanage CD, Pieris M (2015) A physico-chemical analysis of coconut shell powder. Procedia Chem 16:222–228. https://doi.org/10.1016/j.proche.2015.12.045
34. Silva JPC, Rocha RG, Siqueira GP et al (2025) Bio-based plasticizer Babassu oil for custom-made conductive additive-manufacturing filaments: towards 3D-printed electrodes applied to cocaine detection. Microchim Acta 192:47. https://doi.org/10.1007/s00604-024-06910-3
35. Crapnell RD, Kalinke C, Silva LRG et al (2023) Additive manufacturing electrochemistry: an overview of producing bespoke conductive additive manufacturing filaments. Mater Today 71:73–90. https://doi.org/10.1016/j.mattod.2023.11.002
36. Arantes IVS, Crapnell RD, Bernalte E et al (2023) Mixed graphite/carbon black recycled PLA conductive additive manufacturing filament for the electrochemical detection of oxalate. Anal Chem 95:15086–15093. https://doi.org/10.1021/acs.analchem.3c03193
37. Protopasta Conductive filament. https://proto-pasta.com/products/conductive-pla. Accessed 1 Dec 2024
38. Sant'Anna MVS, Carvalho SWMM, Gevaerd A et al (2020) Electrochemical sensor based on biochar and reduced graphene oxide nanocomposite for carbendazim determination. Talanta 220:121334. https://doi.org/10.1016/j.talanta.2020.121334
39. Gnanasekaran K, Heijmans T, van Bennekom S et al (2017) 3D printing of CNT- and graphene-based conductive polymer nanocomposites by fused deposition modeling. Appl Mater Today 9:21–28. https://doi.org/10.1016/j.apmt.2017.04.003
40. Terzioğlu P, Parın FN (2020) Biochar reinforced polyvinyl alcohol/corn starch biocomposites. Süleyman Demirel Üniversitesi Fen Bilimleri Enstitüsü Dergisi 24:35–42. https://doi.org/10.19113/sdufenbed.568229
41. Arrigo R, Bartoli M, Malucelli G (2020) Poly(lactic acid)–biochar biocomposites: effect of processing and filler content on rheological, thermal, and mechanical properties. Polymers (Basel) 12:892. https://doi.org/10.3390/polym12040892
42. Rocha DP, Rocha RG, Castro SVF et al (2022) Posttreatment of 3D-printed surfaces for electrochemical applications: a critical review on proposed protocols. Electrochem Sci Adv 2. https://doi.org/10.1002/elsa.202100136
43. Richter EM, Rocha DP, Cardoso RM et al (2019) Complete additively manufactured (3D-printed) electrochemical sensing platform. Anal Chem 91:12844–12851. https://doi.org/10.1021/acs.analchem.9b02573
44. Rocha DP, Ataide VN, de Siervo A et al (2021) Reagentless and sub-minute laser-scribing treatment to produce enhanced disposable electrochemical sensors via additive manufacture. Chem Eng J 425:130594. https://doi.org/10.1016/j.cej.2021.130594
45. Carvalho MS, Rocha RG, Nascimento AB et al (2024) Enhanced electrochemical performance of 3D-printed electrodes via blue-laser irradiation and (electro)chemical treatment. Electrochim Acta 506:144995. https://doi.org/10.1016/j.electacta.2024.144995
46. Rocha RG, Cardoso RM, Zambiazi PJ et al (2020) Production of 3D-printed disposable electrochemical sensors for glucose detection using a conductive filament modified with nickel microparticles. Anal Chim Acta 1132:1–9. https://doi.org/10.1016/j.aca.2020.07.028
47. Yan T, Li R, Li Z (2014) Nickel–cobalt layered double hydroxide ultrathin nanoflakes decorated on graphene sheets with a 3D nanonetwork structure as supercapacitive materials. Mater Res

Bull 51:97–104. https://doi.org/10.1016/j.materresbull.2013.11.044
48. Foster CW, Elbardisy HM, Down MP et al (2020) Additively manufactured graphitic electrochemical sensing platforms. Chem Eng J 381:122343. https://doi.org/10.1016/j.cej.2019.122343
49. Stefano JS, Guterres e Silva LR, Rocha RG et al (2022) New conductive filament ready-to-use for 3D-printing electrochemical (bio)sensors: towards the detection of SARS-CoV-2. Anal Chim Acta 1191:339372. https://doi.org/10.1016/j.aca.2021.339372
50. Crapnell RD, Arantes IVS, Camargo JR et al (2024) Multi-walled carbon nanotubes/carbon black/rPLA for high-performance conductive additive manufacturing filament and the simultaneous detection of acetaminophen and phenylephrine. Microchim Acta 191:96. https://doi.org/10.1007/s00604-023-06175-2
51. Silva LRG, Stefano JS, Crapnell RD et al (2023) Additive manufacturing of carbon black immunosensors based on covalent immobilization for portable electrochemical detection of SARS-CoV-2 spike S1 protein. Talanta Open 8:100250. https://doi.org/10.1016/j.talo.2023.100250
52. Zhang D, Chi B, Li B et al (2016) Fabrication of highly conductive graphene flexible circuits by 3D printing. Synth Met 217:79–86. https://doi.org/10.1016/j.synthmet.2016.03.014
53. Rymansaib Z, Iravani P, Emslie E et al (2016) All-polystyrene 3D-printed electrochemical device with embedded carbon nanofiber-graphite-polystyrene composite conductor. Electroanalysis 28:1517–1523. https://doi.org/10.1002/elan.201600017
54. Dettlaff A, Rycewicz M, Ficek M et al (2022) Conductive printable electrodes tuned by boron-doped nanodiamond foil additives for nitroexplosive detection. Microchim Acta 189:270. https://doi.org/10.1007/s00604-022-05371-w
55. Wang J, Wang S (2019) Preparation, modification and environmental application of biochar: a review. J Clean Prod 227:1002–1022. https://doi.org/10.1016/j.jclepro.2019.04.282
56. Kalderis D, Kayan B, Akay S et al (2017) Adsorption of 2,4-dichlorophenol on paper sludge/wheat husk biochar: process optimization and comparison with biochars prepared from wood chips, sewage sludge and hog fuel/demolition waste. J Environ Chem Eng 5:2222–2231. https://doi.org/10.1016/j.jece.2017.04.039
57. Guo L, Zhao B, Hao L et al (2022) An electrochemical sensor based on MOF-derived porous carbon/graphene composite for sensitive determination of carbendazim. Microchim Acta 189:454. https://doi.org/10.1007/s00604-022-05526-9
58. Yola ML (2022) Carbendazim imprinted electrochemical sensor based on CdMoO4/g-C3N4 nanocomposite: application to fruit juice samples. Chemosphere 301:134766. https://doi.org/10.1016/j.chemosphere.2022.134766
59. Crapnell RD, Adarakatti PS, Banks CE (2023) Electroanalytical overview: the sensing of carbendazim. Anal Methods 15:4811–4826. https://doi.org/10.1039/D3AY01053H
60. Zimmerman AR, Gao B, Ahn M-Y (2011) Positive and negative carbon mineralization priming effects among a variety of biochar-amended soils. Soil Biol Biochem 43:1169–1179. https://doi.org/10.1016/j.soilbio.2011.02.005
61. Suresh I, Selvaraj S, Nesakumar N et al (2021) Nanomaterials based non-enzymatic electrochemical and optical sensors for the detection of carbendazim: a review. Trends Environ Anal Chem 31:e00137. https://doi.org/10.1016/j.teac.2021.e00137
62. Elgrishi N, Rountree KJ, McCarthy BD et al (2018) A practical beginner's guide to cyclic voltammetry. J Chem Educ 95:197–206. https://doi.org/10.1021/acs.jchemed.7b00361
63. Bard AJ, Faulkner LR, White HS (2022) Electrochemical methods: fundamentals and applications. John Wiley & Sons
64. Chen X, Li W, Lu C et al (2022) Highly sensitive electrochemical detection of carbendazim residues in water by synergistic enhancement of nitrogen-doped carbon nanohorns and polyethyleneimine modified carbon nanotubes. Sci Total Environ 851:158324. https://doi.org/10.1016/j.scitotenv.2022.158324
65. Derbalah A, Chidya R, Kaonga C et al (2020) Carbaryl residue concentrations, degradation, and major sinks in the Seto Inland Sea, Japan. Environ Sci Pollut Res 27:14668–14678. https://doi.org/10.1007/s11356-020-08010-0
66. Kalinke C, de Oliveira PR, Neumsteir NV et al (2022) Influence of filament aging and conductive additive in 3D printed sensors. Anal Chim Acta 1191:339228. https://doi.org/10.1016/j.aca.2021.339228
67. Williams RJ, Brine T, Crapnell RD et al (2022) The effect of water ingress on additively manufactured electrodes. Mater Adv 3:7632–7639. https://doi.org/10.1039/D2MA00707J
68. França RF, de Oliveira HPM, Pedrosa VA, Codognoto L (2012) Electroanalytical determination of carbendazim and fenamiphos in natural waters using a diamond electrode. Diam Relat Mater 27–28:54–59. https://doi.org/10.1016/j.diamond.2012.05.010
69. Anshori I, Nuraviana Rizalputri L, Rona Althof R et al (2021) Functionalized multi-walled carbon nanotube/silver nanoparticle (f-MWCNT/AgNP) nanocomposites as non-enzymatic electrochemical biosensors for dopamine detection. Nanocomposites 7:97–108. https://doi.org/10.1080/20550324.2021.1948242
70. Asrafali SP, Periyasamy T, Kim SC, Lee J (2024) Advanced electrochemical monitoring of carbendazim fungicide in foods using interfacial superassembly of NRPC/NiMn frameworks. Biosensors (Basel) 14:474. https://doi.org/10.3390/bios14100474
71. Silva LRG, Stefano JS, Crapnell RD et al (2023) Additive manufactured microfluidic device for electrochemical detection of carbendazim in honey samples. Talanta Open 7:100213. https://doi.org/10.1016/j.talo.2023.100213
72. Guterres Silva LR, Santos Stefano J, Cornélio Ferreira Nocelli R, Campos Janegitz B (2023) 3D electrochemical device obtained by additive manufacturing for sequential determination of paraquat and carbendazim in food samples. Food Chem 406:135038. https://doi.org/10.1016/j.foodchem.2022.135038
73. de Silva JOS, dos Santos JF, Granja HS et al (2024) Simultaneous determination of carbendazim and carbaryl pesticides in water bodies samples using a new voltammetric sensor based on Moringa oleifera biochar. Chemosphere 347:140707. https://doi.org/10.1016/j.chemosphere.2023.140707
74. INMETRO, Sobre O, De V, Analíticos M Coordenação Geral de Acreditação. Accessed Apr 2025